Photothermoelectric detection of gold oxide non-

thermal decomposition

Xifan Wang<sup>1</sup>, Charlotte I. Evans<sup>2</sup>, Douglas Natelson\*,1,2,3

<sup>1</sup>Department of Materials Science and NanoEngineering, Rice University, 6100 Main St.,

Houston, TX 77005, United States

<sup>2</sup>Department of Physics and Astronomy, Rice University, 6100 Main St.,

Houston, TX 77005, United States

<sup>3</sup>Department of Electrical and Computer Engineering, Rice University, 6100 Main St., Houston,

TX 77005, United States

ABSTRACT: A thin coating of gold oxide, metastable at room temperature, can be formed by

placing gold in a strongly oxidizing environment such as an oxygen plasma. We report scanning

photovoltage measurements of lithographically defined gold nanowires subsequent to oxygen

plasma exposure. Photovoltages are detected during the first optical scan of the devices that are

several times larger than those mapped on subsequent scans. The first-scan enhanced photovoltage

correlates with a reduction of the electrical resistance of the nanostructure back to pre-oxygen-

exposure levels. Repeating oxygen plasma exposure "reinitializes" the devices. These combined

photovoltage and transport measurements imply that the enhanced photovoltage results from the

1

photothermoelectric response of a junction between Au and oxidized Au, with optically driven decomposition of the oxide. Comparisons with the known temperature dependent kinetics of AuOx decomposition suggest that the light-driven decomposition is not a purely thermal effect. These experiments demonstrate that combined optical and electronic measurements can provide a window on surface-sensitive photochemical processes.

KEYWORDS: photothermoelectric, plasmon, surface chemistry, nanowire, laser heating, gold oxide

Gold is a metal of choice for many electronics, plasmonics, and surface functionalization applications, thanks in part to its high electrical conductivity and comparative lack of reactivity with atmospheric oxygen. When exposed to an extremely oxidizing environment, however, it is possible to form metastable gold oxide. The presence of such an oxide can be determined directly via x-ray photoemission spectroscopy<sup>1-3</sup>, and indirectly through changes in work function<sup>4</sup>, electrical resistivity<sup>5</sup>, and electrochemical response<sup>6</sup>. This oxide is known to decompose on the timescale of minutes at temperatures above 150 C, with a characteristic energy scale for the kinetics of around 0.6 eV.<sup>2</sup>

Combining electronic measurements with optical excitation has enabled scanning photothermoelectric characterization of electronic nanostructures. 7-10 A focused laser may be raster scanned over the sample as a scannable heat source, with the measured open circuit photovoltage providing a means of assessing the integrated thermoelectric response. Recent experiments on Au nanowires have revealed a surprising spatial dependence of the photothermoelectric response even in metal nanowires with sheet resistances low compared to

the resistance quantum,<sup>8</sup> ascribed to local variations of the Seebeck coefficient due to the granular structure of the material.

The thermoelectric response of nanostructures can be sensitive to surface conditions, as interfacial scattering affects both the energy-dependent electronic conductivity (a key ingredient of the Mott-Gurney component of the Seebeck response<sup>11</sup>) and phonon scattering. The formation of a surface oxide can change the electronic structure and work function of the Au interface, modify the surface scattering of electrons, and alter the local strain due to surface deformation.

Here we report scanning photovoltage measurements in lithographically defined Au nanowires that are consistent with the optically induced decomposition of a surface layer of AuOx. Nanowires 10-20 microns in length are exposed to an O<sub>2</sub> plasma, resulting in an increase of their electrical resistance by several percent. A single room temperature scanning steady-state photovoltage measurement of a nanowire using a 785 nm diode laser (continuous wave) causes the nanowire to revert to its lower resistance, while yielding a comparatively large "first-scan" photovoltage during the scan. Subsequent scans show spatially varying photothermoelectric response as in previous experiments. Re-exposure to oxygen plasma restores the nanowire to a higher resistance state with an associated large photovoltage upon initial scanning. Based on the systematics, we propose that laser exposure is modifying the nanowire surface by driving decomposition of AuOx, and the photovoltage results from the photothermoelectric response of the boundary between Au and Au+AuOx. Within this picture, the temperature dependence and comparison with known thermal decomposition of AuOx and the laser-driven temperature increase of the metal show that the optically driven decomposition process is not purely thermal.

These experiments demonstrate nanostructure-based optoelectronic detection of an optically driven surface chemistry process.

The devices studied in this work were modified gold "bowtie" thin film devices measured in previous works<sup>12-13</sup> which consisted of an extended nanowire (10 um long/120 nm wide, 1nm Ti/14 nm Au thick) between two "fan out" electrodes on 300 nm SiO<sub>2</sub>/Si substrates, as shown in Figure 1. Using a home-built scanning microscope (see Experimental Methods section), a focused 785 nm CW laser beam was raster-scanned along the nanowire to serve as a local heating source. Measurements were taken at room temperature and in high vacuum unless otherwise specified. Similar to previous works<sup>7-8</sup>, using an optical chopper to modulate the intensity and lock-in detection of the resulting open-circuit photovoltage, the open circuit photovoltage of the entire device was measured as a function of laser position. The photovoltage results from the photothermoelectric (PTE) response of the device as it is locally heated by the beam, enabling spatial PTE voltage mapping. The thermoelectric voltage difference between the ends of the wire, which are kept at identical temperatures, is given by  $V = \int_0^l S(x, T) \nabla T(x) dx$ , where S is the location- and temperature-dependent Seebeck coefficient of the material, T(x) is the local temperature, which is spatially inhomogeneous because of the optical heating, and l is the length of the wire, defined as the length of the region of constant width. Previous bolometric measurements based on the temperature-dependent resistivity of the wires have shown that the maximum nanowire temperature increase under the focused laser spot, when the substrate is at room temperature, is several Kelvin<sup>12-13</sup>.

At the nanoscale, the electronic contribution to S can be locally modified by changes in the electron mean free path. When boundary scattering of carriers is significant, changes in

sample dimensions can thus act as effective thermocouples. The junction between each end of the nanowire and the fan-out electrodes acts as a single-metal thermocouple due to the differences of Seebeck coefficients at each location<sup>14-15</sup>; when the laser is incident on those locations, a measureable voltage can be detected 7-8. When the laser is positioned in the middle of the nanowire, the temperature distribution and the device geometry are symmetric. Considering only these two factors, no PTE voltage would be expected. However, due to intrinsic material variation within the nanowire, including grain boundaries, local strain variation, etc., variation in the local S produces effective thermocouples across the nanowire, resulting in a strong spatial dependence of the PTE magnitude and sign. The spatial pattern of the PTE voltage magnitude and sign as a function of laser position is unique to each device. Previous work<sup>8</sup> discusses the possible mechanisms behind the local S variation in more detail. The Mott-Jones equation shows that the Seebeck coefficient is dependent on the electrical conductivity of the material and therefore, the electronic mean free path. At the nanoscale, the specific value of the Seebeck coefficient is determined by the details of the charge carrier transport through the material. Because the metal films are polycrystalline, deposited using evaporation, S can vary due to dispersity of grain sizes, defects, impurities, crystallographic orientations, and surface scattering. This opens the possibility of modifying the PTE response via surface treatment.

Devices were first treated with O<sub>2</sub> plasma to clean the surface to minimize any residual surface contamination from fabrication and immediately placed in the high vacuum cryostation for measurement. An interesting phenomenon was observed from the first scan after O<sub>2</sub> plasma exposure: the first scan's spatial map shows a relatively large PTE voltage along the nanowire of only one sign. Subsequent scans reverted to the previously observed PTE voltage distributions with marked spatial variation and changing sign as shown in Figure 2a. This procedure could be

repeated many times, with a fresh O<sub>2</sub> plasma exposure "reinitializing" the device. the first postplasma scan showing a comparatively uniform, large photovoltage, and subsequent scans showing the sample-specific spatially varying PTE voltage pattern (Figure 2b). Below we refer to these as "later-scan" conditions.

The fact that the plasma treatment involves oxygen appears to be crucial. Devices treated with nitrogen plasma in the same plasma cleaner with the same pressure and power conditions did not show the post-O<sub>2</sub>-plasma photovoltage effect. Instead, N<sub>2</sub>-exposed devices had the same PTE spatial pattern as the non-O<sub>2</sub>-exposed or later-scan O<sub>2</sub>-exposed devices (see Supporting Information Figure S1). Further, since both plasma treatments kinetically remove surface contamination, the fact that the N<sub>2</sub> and O<sub>2</sub> exposed devices respond differently makes it unlikely that the post-O<sub>2</sub> plasma photovoltage results from post-cleaning contamination of the surface due to contaminants within the measurement chamber. The measurements are conducted at a relatively high vacuum (10<sup>-5</sup>~10<sup>-6</sup> Torr). We also note that measurements performed at atmospheric pressure, when adventitious surface adsorbates should be present, show the same sample-specific PTE spatial pattern as the un-treated and later-scan devices.

Metastable gold oxide species can form in a strong oxidation environment such as ozone. Therefore, cleaning the device with O<sub>2</sub> plasma may result in a thin layer of gold oxide (AuO<sub>x</sub>) on the surface. Two-terminal resistance measurements were taken before and after plasma cleaning (Support Information Table 1). As reported previously, the room temperature sheet resistance of the nanowire film is around 6 Ohms. Immediately after O<sub>2</sub> plasma cleaning, the resistance of the nanowire noticeably increases by ~5%. In contrast, no resistance change is detected after cleaning with N<sub>2</sub> plasma. After the first scan after O<sub>2</sub> plasma cleaning, the device resistance turns to the original, lower value. These resistance changes suggest the gold surface may have

been oxidized via O<sub>2</sub> plasma. The few-percent resistance change is compatible with the high resistivity of gold oxide<sup>5</sup> and a corresponding reduction in effective conducting cross-section by a few percent, and therefore an effective reduction in film thickness of ~ 0.7 nm, comparable to a couple of Au atomic diameters. This is comparable to the thickness of AuOx previously produced under UV/ozone<sup>1</sup>. Gold oxide is metastable<sup>16</sup> and can be completely decomposed at 100 °C in 1 hour and at room temperature after few days, respectively<sup>2</sup>. X-ray photoemission spectroscopy (XPS) shows indications of surface oxidation in a large-area Au film prepared identically to the nanowire devices (Figure S3).

Summarizing, O<sub>2</sub> plasma exposure increases nanowire resistance, and 785 nm laser exposure restores the nanowire to its initial low resistance state. Photovoltage measurements during that initial optical scan show a relatively uniform voltage, while subsequent scans show the spatial variation in PTE voltage previously reported. This procedure may be repeated many times. These results suggest a possible mechanism: Oxygen treatment creates a thin surface AuOx layer, and focused laser exposure during the first photovoltage scan decomposes the AuOx. The measured photovoltage in that first scan in this picture would result from the thermoelectric response of the boundary between the unoxidized Au nanowire and the remaining AuOx-coated nanowire.

If this hypothesis is correct, then the polarity of the measured first-scan photovoltage should depend on the direction of the laser scan during the photovoltage measurement. The laser heating should always be on the unoxidized Au side of the Au/Au+AuOx junction, and the orientation of that junction relative to the measurement electrodes depends on the scan direction. Figure 3 shows exactly this result: The first scan's photovoltage polarity changes with scanning direction, whereas subsequent scans remain unaffected.

Similarly, if the first-scan photovoltage is a PTE voltage generated at the Au/Au+AuOx boundary, then first-scan illumination in the center of one of the large pads should produce no measurable response, because that boundary would be entirely surrounded by metal to short out such a voltage. This, too, is consistent with the measurements, which show no photovoltage response on the big pads away from the nanowire, on the first or subsequent scans.

We also examined the temperature dependence and rate of the light-driven process taking place during the first scan. Each pixel in the photovoltage scans is acquired in 0.3 second. The thermal decomposition kinetics of AuOx have been studied in detail<sup>2</sup>, and temperatures well in excess of 150 °C would be needed for purely thermally activated AuOx decomposition on that timescale. Since local optically driven temperature increases of the metal in this configuration are known at room temperature to be 10 K at the most extreme<sup>12-13</sup>, some nonthermal mechanism must be at work in the optically driven surface modification, or the kinetics of AuOx decomposition would have to be considerably more rapid for very thin oxide layers. The persistence of the first-scan effects in samples that have spent hours at room temperature argues against that latter possibility.

One possibility to consider is a process driven by photo-produced hot electrons<sup>17-18</sup>. Due to the device geometry, the gold nanowire has a strong local surface plasmon resonance under illumination of the 785 nm wavelength laser in the transverse polarization (along the short axis of the nanowire),<sup>12, 19</sup> and plasmon excitation is one means of hot carrier generation, in addition to ordinary optical absorption. If hot carrier generation is the sole mechanism for the optically driven surface chemistry at work here, the first-scan photovoltage and resistivity reduction should also be observed at low substrate temperatures. We find (see Supporting Information Figure S2) that at temperatures below 270 K, there is neither a first-scan photovoltage effect nor

an optically driven change in device resistance. After warming the devices previously scanned at lower temperatures, both effects are seen in the first optical scan taken above 270 K. These results from low temperatures indicate that the dominant mechanism for the surface modification is not purely based on photoexcited hot carriers, and that another mechanism must come into play.

Figure 4 shows the results of additional experiments performed at room temperature to understand the process at work here. After oxygen plasma exposure, the laser is focused on the middle of the nanowire while measuring the PTE voltage. As shown in Figure 4, the magnitude of the PTE voltage dropped dramatically in the first few seconds and slowly dropped to a stable value after about 300 seconds. Subsequent scans show a PTE voltage pattern typical of a later-scan normal device, and the device resistance has returned to its lower value. These results indicate that the likely AuOx has decomposed across the whole nanowire after a certain time even though the laser is only focused on the middle of the nanowire. Considering that the spot size  $(1.8 \ \mu\text{m})$  of laser is much smaller than the nanowire  $(10 \ \mu\text{m})$ , the rapid decrease in PTE voltage magnitude could be due to gold oxide decomposition within the laser spot area. The subsequent slow decrease of PTE voltage magnitude may then be due to the gold oxide decomposition on the rest of nanowire not directly heated by the laser.

From the above results, the apparent AuOx decomposition on the nanowire is strongly and abruptly inhibited at lower temperatures and can be triggered by focusing the laser on only a fraction of the nanowire. While it is speculative at this point, it is important to consider that residual gases could play some role, despite the relatively high chamber vacuum. When the system temperature is decreased, residual gases condense on the coldest portions of the chamber. This may explain the comparatively sudden suppression of the light-driven decomposition with

decreasing temperature. The present chamber configuration makes *in situ* monitoring of residual gas composition impractical, so experiments testing for this issue will require further developments. Next steps to better understand the mechanism at work here include examining the spectroscopic dependence of the photovoltage/resistance changes on incident wavelength, and *in situ* monitoring of residual gas composition within the chamber, both of which are quite technically challenging.

Photovoltage mapping of gold nanostructures has revealed a light-driven photovoltage response and reduction in electrical resistance in nanowires previously immediately exposed to an oxygen plasma environment. These effects can be observed repeatedly if the devices are again subjected to oxygen plasma, strongly suggesting that metastable AuOx and its light-driven decomposition are responsible. The systematics imply that the photovoltage originates from PTE response of the boundary between Au and Au+AuOx. The observed temperature dependence and timescale for light-driven surface modification, combined with the known kinetics for AuOx decomposition, show that the decomposition here is not purely photothermal, and may result from catalytic processes involving residual gases within the measurement system. While raising questions about detailed mechanisms beyond the scope of the present study, these experiments demonstrate the optoelectronic detection of a light-driven surface chemical process in individual nanostructures.

**Methods**: All devices were fabricated on n-type Si wafers with a 300 nm of thermally grown oxide. Prior to the e-beam lithography for nanowire device fabrication, a set of Au/Ti contact pads for wire bonding was evaporated on the substrates using a shadow mask. Metallization

(Au/Ti) layers were deposited using an e-beam evaporator. The thickness of the Au nanowire and connecting electrodes was 14 nm with an additional 1 nm Ti as an adhesion layer. Each chip contained 24 devices with a shared ground. The total number of devices investigated during this project is 86. The results selected for demonstration represent a typical sample behavior. Plasmatreated samples were prepared by using plasma cleaner (Harrick Plasma) at 18W with O<sub>2</sub> pressure at 1 mbar for 3 minutes. For the N<sub>2</sub> plasma treatment, the same conditions were used but with N<sub>2</sub> feed gas. A homebuilt scanning laser microscope with the ability to record spatially resolved photothermoelectric voltage was used to perform the experiments. The samples were kept under high vacuum of the closed-cycle optical cryostat (Montana Instruments). A mechanical chopper at a frequency of 287 Hz was used to modulate laser light for lock-in amplifier voltage measurement. Unless specially noted, the PTE voltage distributions are recorded with laser polarization perpendicular to the long dimensions of the nanowire (angle assignment of 90°) to provide maximum heating. The open circuit voltage was measured using an SR560 voltage preamplifier. Experiments were conducted with 14 mW laser power recorded at the sample, unless specially noted. The amplitude and sign of the photovoltage were consistent with the voltage maps acquired in previous experiments on similar device configurations.

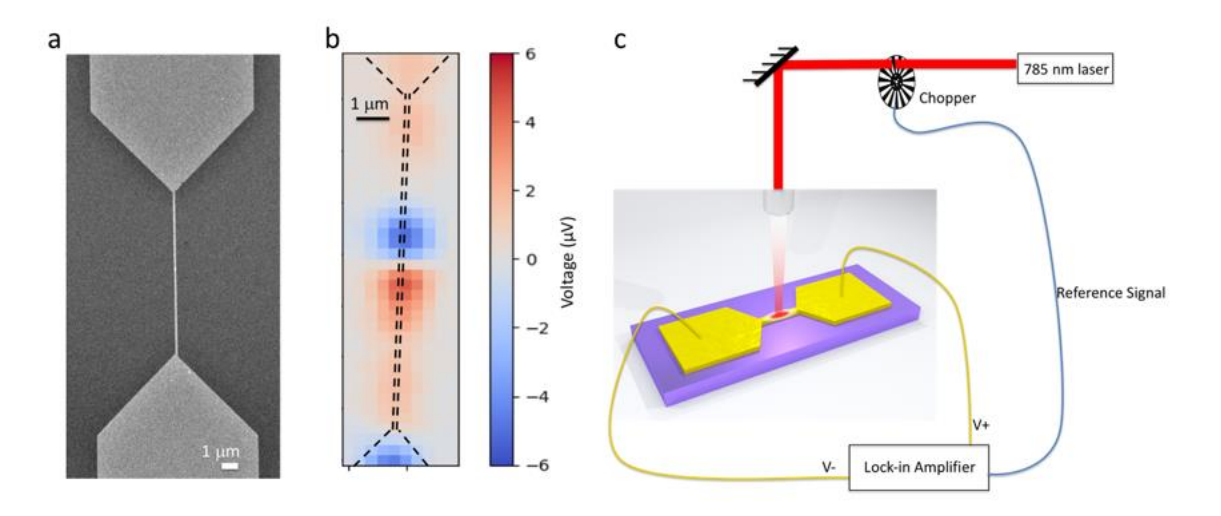


**Figure 1**. PTE voltage maps in Au nanowires. a) Scanning electron microscopy (SEM) image of a typical device. Scale bar is 1μm. The width of the nanowire is about 130 nm, supports a transverse local surface plasmon resonance that may be excited by the 785 nm laser polarized perpendicular to the nanowire. The length of the nanowire is around 10 μm. b) Spatial map of PTE voltage in a typical device. (black dash line indicates the actual device area) c) Schematic of the experimental approach for measuring open-circuit photovoltage.

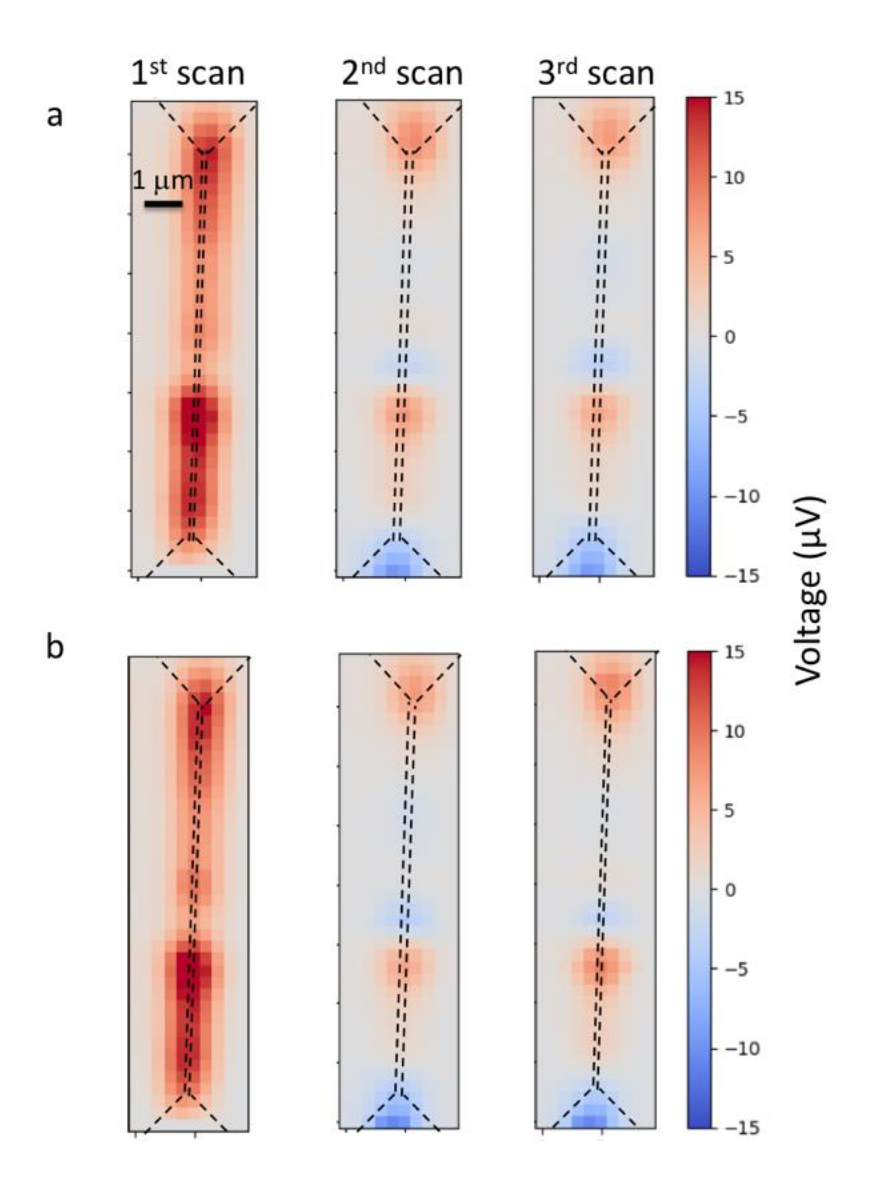


**Figure 2**. PTE voltage map for AuOx Device. a) PTE voltage mapping for oxygen plasma treated device (from left to right indicates the scan sequence). b) Same device showing the reproducibility of the phenomena upon repeated oxygen plasma exposure and subsequent remeasurement.

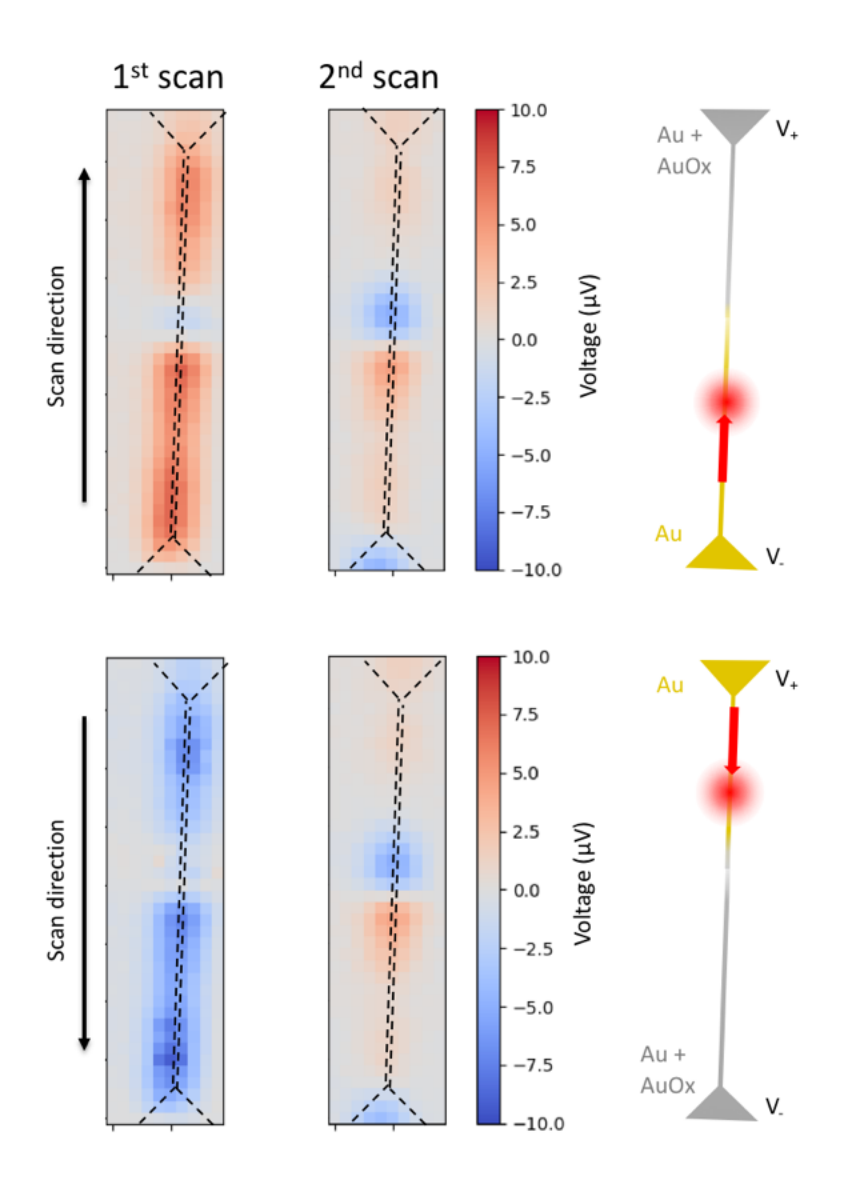
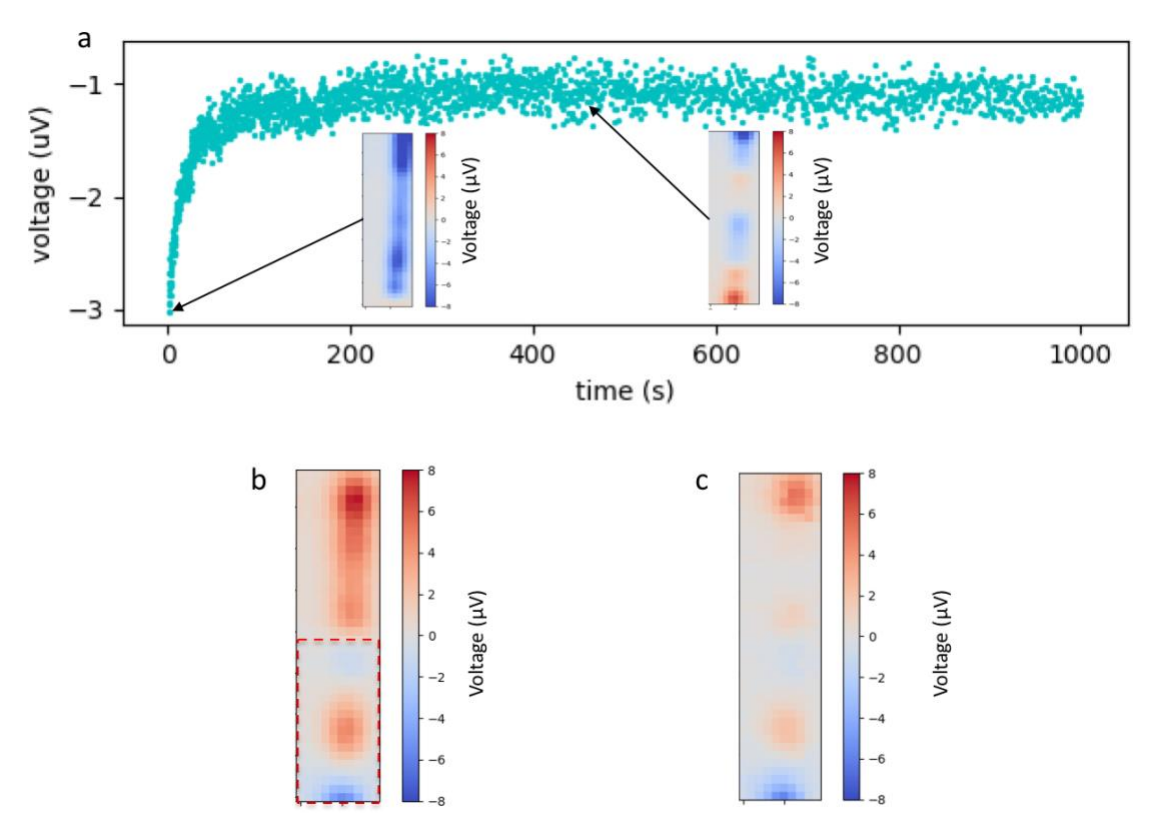


Figure 3. PTE voltage maps for different scan directions. Top row: First and second scan mapping for oxygen plasma treated device while laser scanned from bottom to top with bottom electrode defined as ground. Bottom row: PTE voltage mapping for same device (after retreatment with oxygen plasma) with laser scanned from top to bottom, and bottom electrode defined as ground. Diagrams at right illustrate how the opposite polarities of first-scan photovoltages can be explained in terms of the reversed symmetry (relative to the voltage leads) of the heating of the Au/Au+AuOx boundary.



**Figure 4**. Top panel shows PTE voltage vs. time by focusing laser at a fixed position. Insets indicate the PTE mapping of a freshly oxygen plasma treated device (left) and a scan after focusing the laser on the device center for several minutes. b) PTE voltage map of an AuOx device with bottom half bottom have been previously scanned by laser (red dash line indicates the scanned area). c) PTE voltage map of the device after acquiring the scan in panel b.

**Supporting Information**. The Supporting Information is available free of charge via the Internet at http://pubs.acs.org.

#### **Corresponding Author**

\*To whom correspondence should be addressed. E-mail: <u>natelson@rice.edu</u>

#### **Author Contributions**

XW performed the sample fabrication and measurements. CIE and XW developed aspects of the measurement system. All authors contributed to the analysis and manuscript writing. All authors have given approval to the final version of the manuscript.

#### **ACKNOWLEDGMENT**

DN, XW, and CIE acknowledge support from Robert A. Welch Foundation Grant C-1636. DN and XW acknowledge further support from NSF award ECCS-1704625.

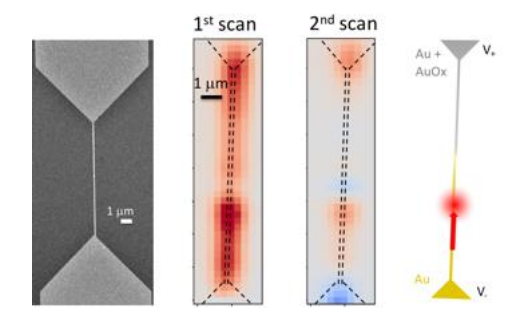
#### **REFERENCES**

- 1. Krozer, A.; Rodahl, M., X-ray photoemission spectroscopy study of UV/ozone oxidation of Au under ultrahigh vacuum conditions. *Journal of Vacuum Science & Technology A* **1997,** *15* (3), 1704-1709.
- 2. Tsai, H.; Hu, E.; Perng, K.; Chen, M.; Wu, J.-C.; Chang, Y.-S., Instability of gold oxide Au2O3. *Surface Science* **2003**, *537* (1), L447-L450.
- 3. Tchaplyguine, M.; Mikkelä, M.-H.; Zhang, C.; Andersson, T.; Björneholm, O., Gold Oxide Nanoparticles with Variable Gold Oxidation State. *The Journal of Physical Chemistry C* **2015**, *119* (16), 8937-8943.
- 4. Rentenberger, S.; Vollmer, A.; Zojer, E.; Schennach, R.; Koch, N., UV/ozone treated Au for air-stable, low hole injection barrier electrodes in organic electronics. *J Appl Phys* **2006**, *100* (5), 053701.

- 5. Machalett, F.; Edinger, K.; Melngailis, J.; Diegel, M.; Steenbeck, K.; Steinbeiss, E., Direct patterning of gold oxide thin films by focused ion-beam irradiation. *Applied Physics A* **2000**, *71* (3), 331-335.
- 6. Steinhauser, B.; Vidal, C.; Barb, R.-A.; Heitz, J.; Mardare, A. I.; Hassel, A. W.; Hrelescu, C.; Klar, T. A., Localized-Plasmon Voltammetry to Detect pH Dependent Gold Oxidation. *The Journal of Physical Chemistry C* **2018**, *122* (8), 4565-4571.
- 7. Zolotavin, P.; Evans, C.; Natelson, D., Photothermoelectric Effects and Large Photovoltages in Plasmonic Au Nanowires with Nanogaps. *J Phys Chem Lett* **2017**, *8* (8), 1739-1744.
- 8. Zolotavin, P.; Evans, C. I.; Natelson, D., Substantial local variation of the Seebeck coefficient in gold nanowires. *Nanoscale* **2017**, *9* (26), 9160-9166.
- 9. Xu, X.; Gabor, N. M.; Alden, J. S.; van der Zande, A. M.; McEuen, P. L., Photo-Thermoelectric Effect at a Graphene Interface Junction. *Nano Lett* **2010**, *10* (2), 562-566.
- 10. Shi, S. F.; Xu, X.; Ralph, D. C.; McEuen, P. L., Plasmon Resonance in Individual Nanogap Electrodes Studied Using Graphene Nanoconstrictions as Photodetectors. *Nano Lett* **2011**, *11* (4), 1814-1818.
- 11. Mott, N. F.; Jones, H., *The Theory of the Properties of Metals and Alloys*. Dover Publications: 1958.
- 12. Herzog, J. B.; Knight, M. W.; Natelson, D., Thermoplasmonics: Quantifying Plasmonic Heating in Single Nanowires. *Nano Lett* **2014**, *14* (2), 499-503.

- 13. Zolotavin, P.; Alabastri, A.; Nordlander, P.; Natelson, D., Plasmonic Heating in Au Nanowires at Low Temperatures: The Role of Thermal Boundary Resistance. *ACS Nano* **2016**, *10* (7), 6972-6979.
- 14. Liu, H.; Sun, W.; Xu, S., An Extremely Simple Thermocouple Made of a Single Layer of Metal. *Adv Mater* **2012**, *24* (24), 3275-3279.
- 15. Szakmany, G. P.; Orlov, A. O.; Bernstein, G. H.; Porod, W., Single-Metal Nanoscale Thermocouples. *IEEE Transactions on Nanotechnology* **2014**, *13* (6), 1234-1239.
- 16. Liu, Y.-L.; Fang, C.-Y.; Yu, C.-C.; Yang, T.-C.; Chen, H.-L., Controllable Localized Surface Plasmonic Resonance Phenomena in Reduced Gold Oxide Films. *Chemistry of Materials* **2014**, *26* (5), 1799-1806.
- 17. Hou, W.; Cronin Stephen, B., A Review of Surface Plasmon Resonance-Enhanced Photocatalysis. *Advanced Functional Materials* **2012**, *23* (13), 1612-1619.
- 18. Brongersma, M. L.; Halas, N. J.; Nordlander, P., Plasmon-induced hot carrier science and technology. *Nat Nanotechnol* **2015**, *10*, 25.
- 19. Herzog, J. B.; Knight, M. W.; Li, Y. J.; Evans, K. M.; Halas, N. J.; Natelson, D., Dark Plasmons in Hot Spot Generation and Polarization in Interelectrode Nanoscale Junctions. *Nano Lett* **2013**, *13* (3), 1359-1364.

# TOC Figure:



## **Supporting Information**

### Photothermoelectric detection of gold oxide non-thermal decomposition

Xifan Wang<sup>1</sup>, Charlotte I. Evans<sup>2</sup>, Douglas Natelson\*,1,2,3

<sup>1</sup>Department of Materials Science and NanoEngineering, Rice University, 6100 Main St.,

Houston, TX 77005, United States

<sup>2</sup>Department of Physics and Astronomy, Rice University, 6100 Main St.,

Houston, TX 77005, United States

<sup>3</sup>Department of Electrical and Computer Engineering, Rice University, 6100 Main St., Houston,

TX 77005, United States

\*To whom correspondence should be addressed. E-mail: <a href="mailto:natelson@rice.edu">natelson@rice.edu</a>

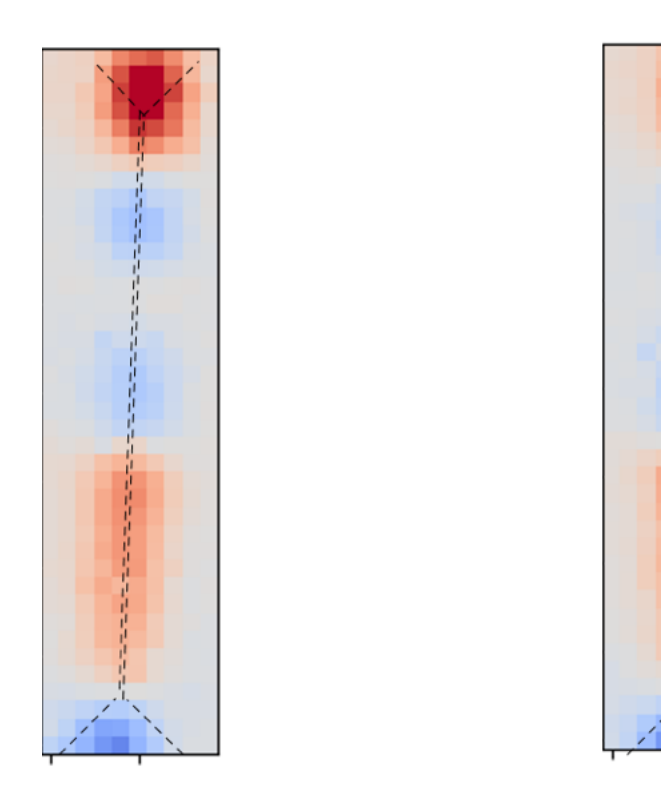


**Figure S1.** Room temperature PTE voltage map for  $N_2$  plasma cleaned device. Left panel is the result from "non-treated" device. Right panel is the same device immediately after exposure to  $N_2$  plasma.

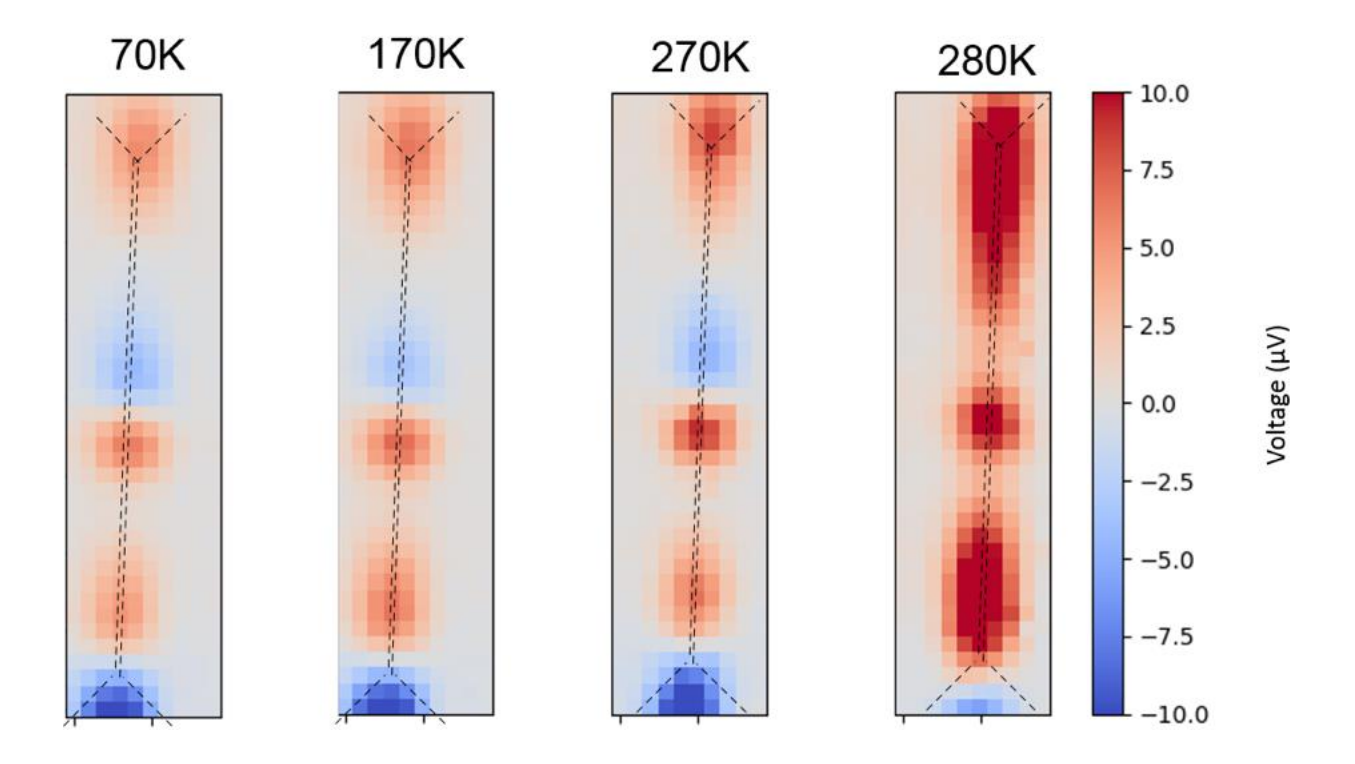


**Figure S2.** PTE voltage map for device exposed to  $0_2$  plasma and immediately cooled to cryogenic temperatures. From left to right: The device was measured at successively increasing temperatures (70K, 170K, 270K, 280K). Observing the "first-scan" photovoltage response requires the temperature to be in excess of 270 K.

| Device No. | Initial R (Ω) | Post-02 plasma R (Ω) | Post "first-scan" R (Ω) |
|------------|---------------|----------------------|-------------------------|
| A.1        | 470.5         | 497.4                | 471.2                   |
| A.2        | 462.9         | 488.3                | 463.1                   |
| A.3        | 468.9         | 495.6                | 469.3                   |
| A.4        | 474.2         | 501.1                | 474.5                   |
| A.5        | 469.7         | 497.2                | 470                     |
| A.6        | 472.4         | 500.3                | 473.2                   |
| B.1        | 451.6         | 475.5                | 451.7                   |
| B.2        | 448.1         | 470.8                | 448.6                   |
| B.3        | 449.5         | 468.9                | 450                     |
| B.4        | 443           | 465.6                | 443.8                   |
| B.5        | 437.3         | 460.2                | 437.9                   |
| B.6        | 441           | 463.4                | 441.3                   |
| C.1        | 453.8         | 476.5                | 454.1                   |
| C.2        | 459.6         | 483.3                | 460                     |
| C.3        | 458.2         | 482.6                | 459.2                   |
| C.4        | 466.4         | 489.6                | 466.8                   |
| C.5        | 463.2         | 486.9                | 463.5                   |
| C.6        | 470.5         | 493.2                | 470.7                   |
| Average    | 458.9         | 482.9                | 459.4                   |

**Table 1**. Two terminal resistance measurements for devices pre-plasma exposure, post- $O_2$ -plasma exposure, and post-"first-scan". Device numbers indicate the devices' numbers from 3 different fabrication batches. Laser exposure during the first-scan restores the original pre- $O_2$  plasma device resistance.

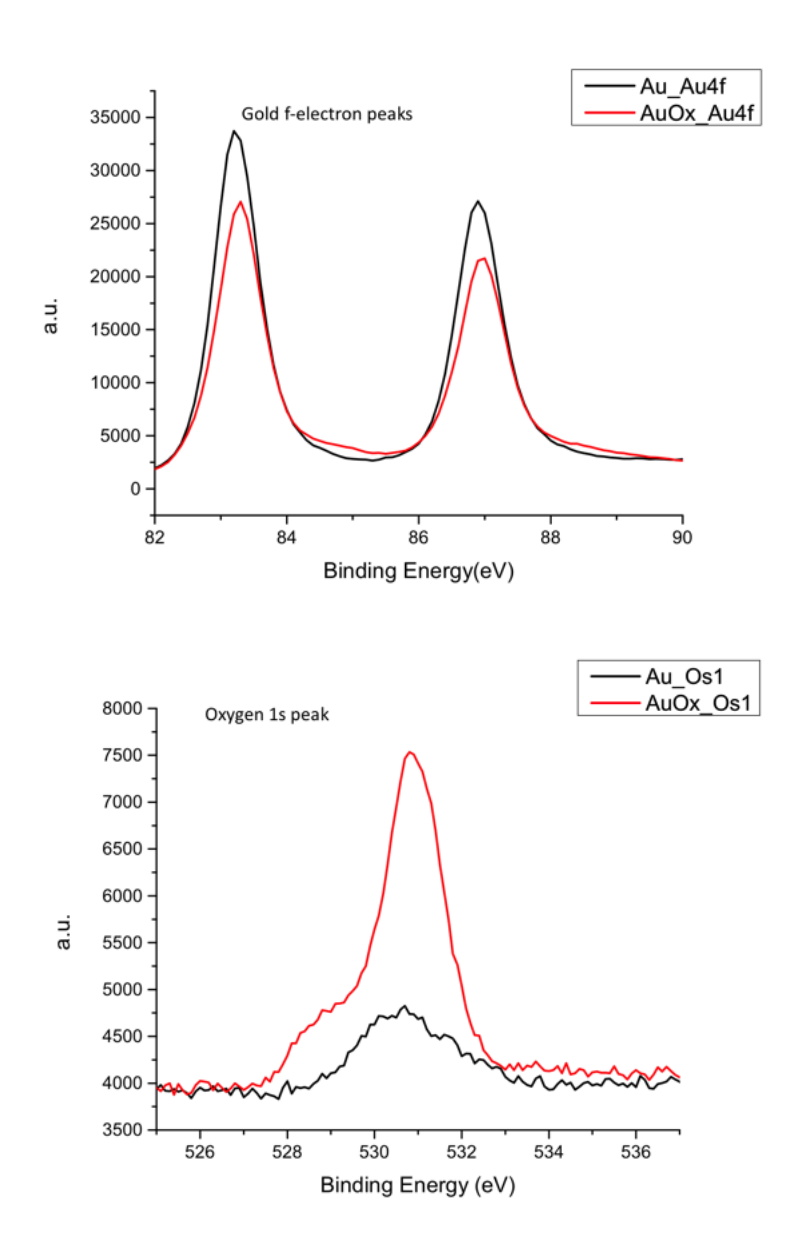


**Figure S3**. X-ray photoemission spectroscopy of a gold film on an oxidized silicon substrate, before and after oxygen plasma exposure identical to the procedure employed for the nanowire samples. Comparing pre- and post-plasma exposure films, post-plasma we find a clear increase in the oxygen signal, and systematic shifts to higher binding energies for the Au f-electron peaks, as well as the development of a shoulder or weak peak between the large peaks. See below. These signatures are similar to those present in other Au films exposed (Tsai al., oxygen plasma et Surf Sci 537, (2003),https://doi.org/10.1016/S0039-6028(03)00640-X, Ref [2] of the main text).